Heat transfer and entropy generation analysis of HFE 7000 based nanorefrigerants

H. U. Helvaci*, Z. A. Khan

Bournemouth University, NanoCorr, Energy and Modelling (NCEM), Faculty of Science and Technology, Bournemouth, BH12 5BB, UK

* Corresponding author: Huseyin Utku Helvaci

Faculty of Science and Technology, Fern Barrow, Talbot Campus, Bournemouth University, Poole, Dorset BH12 5BB

Tel: +44 7473 770009

E-mail address: hhelvaci@bournemouth.ac.uk

Abstract

In this study, two dimensional numerical simulations of forced convection flow of HFE 7000 based nanofluids in a horizontal circular tube subjected to a constant and uniform heat flux in laminar flow was performed by using single phase homogeneous model. Four different nanofluids considered in the present study are Al_2O_3, CuO, SiO_2 and MgO nanoparticles dispersed in pure HFE 7000. The simulations were performed with particle volumetric concentrations of 0, 1, 4 and 6% and Reynolds number of 400, 800, 1200 and 1600. Most of the previous studies on the forced convective flow of nanofluids have been investigated through hydrodynamic and heat transfer analysis. Therefore, there is limited number of numerical studies which include both heat transfer and entropy generation investigations of the convective flow of nanofluids. The objective of the present work is to study the influence of each dispersed particles, their volume concentrations and Reynolds number on the hydrodynamic and thermal characteristics as well as the entropy generation of the flow. In addition, experimental data for Al_2O_3-water nanofluid was compared with the simulation model and high level agreement was found between the simulation and experimental results. The numerical results reveal that the average heat transfer coefficient augments with an increase in Reynolds number and the volume concentration for all the above considered nanofluids. It is found that the highest increase in the average heat transfer coefficient is obtained at the highest volume concentration ratio (6%) for each nanofluids. The increase in the average heat transfer coefficient is found to be 17.5% for MgO-HFE 7000 nanofluid, followed by Al_2O_3-HFE 7000 (16.9%), CuO-HFE 7000 (15.1%) and SiO_2-HFE 7000 (14.6%). However, the results show that the enhancement in heat transfer coefficient is accompanied by the increase in pressure drop, which is about (9.3 - 28.2%). Furthermore, the results demonstrate that total entropy generation reduces with the rising Reynolds number and particle volume concentration for each nanofluid. Therefore, the use of HFE 7000 based

MgO, Al_2O_3, CuO and SiO_2 nanofluids in the laminar flow regime is beneficial and enhances the thermal performance.

Keywords: CFD; nanofluid; heat transfer coefficient; pressure loss; entropy generation

Nomenclature

A	area, m^2	*fr*	frictional
C_p	specific heat, J/kg K	gen	generation
D	diameter, m	*in*	inlet
f	friction factor	*m*	mean
GWP	global warming potential	*nf*	nanofluid
h	heat transfer coefficient, $W/(m^2K)$	*out*	outlet
HFE	hydrofluoroether	*s*	nanoparticle
k	thermal conductivity, W/m K	*th*	thermal
L	length, m	*tot*	total
Nu	Nusselt number	*w*	wall
ODP	ozone depletion potential		
R	radius of the tube, m	*Greek symbols*	
P	pressure, Pa	ρ	density, kg/m^3
q''	heat flux, W/m^2	η	first law efficiency
Re	Reynolds umber	ε	second law efficiency
S	entropy, W/K	μ	dynamic viscosity, kg/m s
T	temperature, K	ϕ	particle volume concentration (%)
u	Velocity in axial direction, m/s		
$\dot{W}$	work rate, W		
Subscripts			
amb	ambient		
ave	average		
bf	base fluid		
f	fluid		

1. Introduction

The low thermal conductivity of traditional fluids for instance, water, mineral oil and ethylene glycol is one of the obstacles to higher compactness and efficiency of heat exchangers [1] and it is crucial to develop more efficient heat transfer fluids with substantially higher thermal conductivity [2]. Therefore, micro/millimetre-sized solid particles which have considerably higher thermal conductivity than those fluids have been suspended in them to cause an enhancement in the thermal conductivity [3, 4]. However, significant problems such as abrasion and clogging were observed when particles of the order of millimetres and micrometres are suspended in a liquid.

Alternatively, nano-sized particles suspended in conventional fluids can provide an improvement in the performance of these fluids. Such novel liquid suspensions that consist of solid particles at nanometric scale are called *nanofluids* and have become popular in terms of its utilisation in various practices such as heat transfer, thermal energy storage and industrial cooling [5, 6]. Nanofluids have superior heat transfer performance than conventional fluids because of the improved effective thermal conductivity of the fluid [7]. As a consequence, several studies have been conducted on the investigation of thermo-physical properties of nanofluids, particularly the effective thermal conductivity and viscosity [8-13]. Superior thermal conductivity and viscosity of nanofluids in comparison to the base fluids were reported in the above studies. However, in addition to the thermo-physical properties, forced convection (laminar and turbulent flow) heat transfer characteristics of nanofluids need to be investigated as it is important for their practical applications [14]. One of the earliest experimental work on forced convection of nanofluids was conducted by Xuan and Li [7]. In their study, Cu-water nanofluid was used to examine the heat transfer process of the nanofluid. They obtained higher heat transfer performance for the nanofluid compared to that of the base liquid. Another experimental study was conducted by Wen et al. [15] where the effect of the laminar flow of water-Al_2O_3 nanofluid was analysed. They stated that the heat transfer rate rose by addition of nanoparticles, especially at the entrance region of the tube. The relation between the heat transfer coefficient and nanoparticle size and Peclet number was studied by Heris et al. [16] for Al_2O_3-water and CuO-water nanofluids in a circular tube.

It was found that the heat transfer coefficient soared with increasing particle size and Peclet number for both nanofluids.

In addition to experimental studies, numerical analysis of forced convection of nanofluids has been of interest to many researchers. Numerical analysis in the literature consists of two different approaches for evaluating the heat transfer correlations of nanofluids which are single phase (homogenous) and two-phase (mixture) models. In the former model, nanofluid is assumed as a single fluid rather than a solid-fluid mixture and it is also assumed that there is no motion slip between particles and fluid. Moraveji et al. [17] numerically studied the convective heat transfer coefficient of Al_2O_3 nanofluid along a tube using single phase model. It was observed that the heat transfer coefficient rose with increasing nanoparticle volume fraction ratio and the Reynolds number. Demir et al. [18] investigated the forced convection flow of nanofluids in a horizontal tube subjected to constant wall temperature. They utilised homogeneous model with two-dimensional equations in order to study the effects of TiO_2 and Al_2O_3 nanoparticles and Reynolds number on the convective heat transfer coefficient, Nusselt number and pressure drop. The results revealed that nanofluids with a higher volume ratio showed a higher improvement of heat transfer rate. Salman et al. [19] investigated the laminar forced convective flow of water based Al_2O_3 and SiO_2 nanofluids numerically. The results indicated that SiO_2-water and Al_2O_3-water nanofluids have better heat transfer properties compared to pure water.

In order to take the effect of nanoparticle chaotic movements into account in single phase model, thermal dispersion approach is proposed by several researchers [20-22]. These researchers also concluded that increasing particle volume concentration enhances the heat transfer rate. Furthermore, the mixture model approach where the interactions between the particle and fluid are considered is also proposed in several numerical analyses in the literature [23-26].

As previously mentioned suspending nano-scale particles in a base fluid enhances the thermal conductivity but also increases the viscosity. An augmentation in the thermal conductivity leads a better heat transfer rate, whereas an increase in the viscosity leads an enhancement in pressure drop. Consequently, the addition of the particles changes the thermophysical properties of a fluid as well as the irreversibility of a system [27]. Entropy generation demonstrates the irreversibility of a system thus, it is important to minimise the entropy generation to obtain better working conditions [28, 29]. As a result, entropy generation analysis has been considered in nanofluid flow analysis in order to find the optimum working conditions by several researchers [27, 30-37]. For instance, Moghaddami et al. [31] studied the estimation of the entropy generation of Al_2O_3 particles suspended in water and ethylene glycol in a circular tube for both laminar and turbulent flows. They revealed that the entropy generation is diminished by the addition of the particles at any Reynolds number for laminar flow. However, for turbulent flow it is stated that utilising the nanoparticles in the base fluid is beneficial only at Reynolds number smaller than 40000. Biancoa et al. [28] studied the numerical entropy generation of Al_2O_3-water nanofluids under the turbulent forced convection flow for fixed Reynolds number, mass flow rate and velocity. Their numerical outcomes reveal that at constant velocity condition, lower concentration of nanoparticles can minimise the total entropy generation. In another study, Saha et al. [33] evaluated the entropy generation of water based TiO_2 and Al_2O_3 nanofluids for turbulent flow in a heated pipe. It was found that there is an optimum Reynolds number where the entropy generation is minimised. They also showed that the use of TiO_2 nanofluid is more beneficial than Al_2O_3 nanofluid.

Hydrofluoroethers (HFEs) which are the new generation refrigerants have zero Ozone Depletion Potential (ODP) and relatively low Global Warming Potential (GWP). Therefore, they have been used in various applications as a replacement to conventional refrigerants such as Chlorofluorocarbons (CFCs) and hydrochlorofluorocarbons (HCFCs) [38]. In addition to that HFE 7100 based nanofluids have been of interest to various researchers in terms of convective heat transfer analysis [39-41]. Previously, HFE 7000 (RE 347mcc) refrigerant has been studied both experimentally and numerically in terms of its utilisation in various solar thermal applications [42, 43]. In this study, laminar forced convection flow characteristics of HFE 7000 (RE 347mcc) based Al_2O_3, SiO_2, CuO and MgO nanofluids in a horizontal tube under constant heat flux is analysed numerically. Single phase homogeneous approach is applied in order to investigate the effects of Reynolds number and particle volume concentration ratio on both the heat transfer coefficient and the pressure drop of each nanofluid. Furthermore, the entropy generation analysis is provided for each nanofluid flow to specify the most beneficial nanofluid with optimum working conditions that minimises the total entropy generation of the flow.

2. Problem definition

In this study, two dimensional, steady state, laminar flow in a circular tube, subjected to constant heat flux is investigated. The geometry of the considered problem is represented in Figure 1. As it can be seen from the figure, the computational domain consists of a tube with a length of 1.2 m and a diameter of 0.00475 m. In the analysis, only the top half of the tube is considered as the flow is presumed to be symmetrical. In the simulations, 1000 W/m^2 constant heat is supplied on the upper wall of the tube. Also, the base and nanofluids enters the tube at temperature of 283K and the pressure of 1 bar. This inlet temperature is chosen due to the HFE 7000 saturation pressure-temperature conditions.

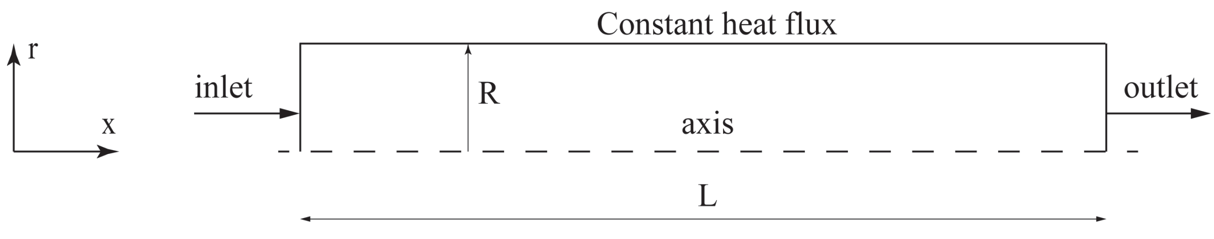

Figure 1 Schematic of the flow domain under consideration

3. Numerical analysis

The defined problem is solved using single phase approach where the base fluid HFE 7000 (RE 347mcc) and the particles are assumed to be in equilibrium and there is no relative velocity between the two of them.

3.1. Mathematical modelling

The following equations (continuity, momentum and energy) for laminar, incompressible flow can be expressed as follows:

Continuity equation:

$$\nabla .\left(\rho_{nf} V\right) = 0 \tag{1}$$

Momentum equation:

$$\nabla .\left(\rho_{nf} V V\right) = -\nabla P + \nabla .\left(\mu_{nf} \nabla V\right) \tag{2}$$

Energy equation:

$$\nabla\left(\rho_{nf} V C_p T\right) = \nabla\left(k_{nf} \nabla T\right) \tag{3}$$

3.2. Thermo-physical properties of nanofluids

The thermal and physical properties of nanofluids are investigated using the formulas below:

The density of nanofluid can be calculated by the equation developed by Pak and Chao [44]:

$$\rho_{nf} = \phi \rho_s + (1 - \phi) \rho_{bf} \tag{4}$$

where ϕ is the nanoparticle volume concentration, ρ_s and ρ_{bf} are the nanoparticle and base fluid densities respectively.

Mass-averaged calculation of specific heat which is based on heat capacity concept of nanofluid is shown below [29]:

$$C_{p,nf} = \frac{\phi(\rho C_p)_s + (1-\phi)(\rho C_p)_{bf}}{\phi\rho_s + (1-\phi)\rho_{bf}} \tag{5}$$

where $C_{p,s}$ and $C_{p,bf}$ are particles and base fluid heat capacity respectively.

Effective thermal conductivity of nanofluid is obtained in the following form [45]:

$$k_{nf} = k_{bf}\frac{[k_s + (n-1)k_{bf} + (n-1)\phi(k_s - k_{bf})]}{[k_s + (n-1)k_{bf} - \phi(k_s - k_{bf})]} \tag{6}$$

where k_{bf} and k_s are the thermal conductivities of the base fluid and solid particles and n = 3 for spherical solid particles.

Dynamic viscosity of nanofluid is estimated by using Einstein's equation which is based on kinetic theory [46]:

$$\mu_{nf} = \mu_{bf}(1 + 2.5\phi) \tag{7}$$

In Equation (7), μ_{nf} and μ_{bf} are the dynamic viscosity of the nanofluid and base fluid respectively.

The thermo-physical properties of two base fluids (water and HFE 7000) and the materials used in this study are given in Table 1.

Table 1 Thermo-physical properties of the base fluids (water and HFE 7000) and the nanoparticles

Fluid/Particle	Density (kg/m^3)	Specific heat (J/kg.K)	Thermal conductivity (W/mK)	Viscosity (kg/m.s)	Reference
Pure water	998.2	4182	0.6	0.001003	[47]
HFE 7000*	1446.1	1204.6	0.079	0.00058	[48]
Al_2O_3	3970	765	40	-	[49]
SiO_2	2200	703	1.2	-	[19]
MgO	3560	955	45	-	[47]
CuO	6500	535.6	20	-	[50]

* The data is taken at 1 bar and 283 K

3.3. *Boundary conditions*

In order to solve the governing equations given above, the appropriate boundary conditions are applied and expressed as follows;

Uniform velocity boundary condition depending on the value of the flow Reynolds number and inlet temperature are defined at the inlet of the tube.

$u(0, r) = U, v(0, r) = 0$

$T(0, r) = T_{in}$

No-slip boundary conditions at the wall ($r = D/2$) is imposed. Therefore, the velocity at the upper wall becomes;

$u(x, R) = v(x, R) = 0$

The upper surface of the tube is subjected to a constant heat flux and it is expressed as;

$$-k_{nf} \left.\frac{\partial T}{\partial r}\right|_{r=R} = q''$$

Finally, at the exit section of the tube pressure outlet condition is applied.

4. Numerical procedure

In this study, the governing equations (continuity, momentum and energy) with appropriate boundary conditions are solved by employing the finite volume solver Fluent 6.3.26 [51]. Second order upwind scheme is applied for solving the convective and diffusive terms. The SIMPLE algorithm is used to model pressure-velocity coupling. The residue of 10^{-6} is defined as convergence criteria for all the dependent variables as mass, velocity and energy.

4.1. Data reduction

The local heat transfer coefficient is expressed as:

$$h(x) = \frac{q''}{T(x)_w - T(x)_{f,m}} \tag{8}$$

where $T(x)_w$ represents the wall temperature at a given location *(x)* along the tube and it is calculated as:

$$T(x, R) = T(x)_w \tag{9}$$

where x represents any given axial position along the tube and R is the radius of the tube. $T(x)_{f,m}$ is the fluid mean temperature at any *(x)*, which can be found via integration:

$$T(x)_{f,m} = \frac{\int_0^R urTdr}{\int_0^R urdr} \tag{10}$$

where u is the velocity in axial *(x)* direction.

The average convective heat transfer coefficient is calculated as:

$$\boldsymbol{h_{ave} = \frac{1}{L}\int_0^L h(x)dx} \tag{11}$$

In addition to heat transfer coefficient, the total entropy generation rate of the fluid flow is evaluated in order to determine the benefits of using nanofluid in terms of thermodynamic analysis. The total entropy generation rate of a flow in a circular tube which consists of two parts: (i) thermal entropy generation (ii) frictional entropy generation is calculated as follows [33]:

$$S_{tot} = \frac{(q'')^2 \pi D^2 L}{Nuk{T_{ave}}^2} + \frac{32\dot{m}^3 fL}{\pi^2 \rho^2 T_{ave} D^5} \tag{12}$$

In Eq. (12), the first term of the left hand side represents the thermal entropy generation and the second term represents the frictional entropy generation.

In the first term, D indicates the diameter of the tube, Nu is the Nusselt number, k and T_{avg} are the thermal conductivity and the average temperature of fluid.

Average Nusselt number and fluid temperature are given by:

$$Nu_{ave} = \frac{h_{ave} D}{k} \tag{13}$$

$$T_{ave} = \frac{T_{in} - T_{out}}{ln\left(\frac{T_{in}}{T_{out}}\right)} \tag{14}$$

In the second term $\dot{m}$ is the flow mass flow rate, f and ρ represent friction factor and the density of fluid respectively.

Friction factor *(f)* can be calculated using the following equation:

$$f = \frac{2 \cdot \Delta P \cdot D}{\rho \cdot V^2 \cdot L} \tag{15}$$

4.2. Grid independency test

A grid independency test is conducted to guarantee the accuracy of the numerical results. Five different sets of uniform grids have been used to check for grid independency. The tests were carried out for both pure water and HFE 7000 at Re = 800 and Re = 1600 for each of the grids. Table 2 shows the comparison of the results for each fluid. It can be seen that the value of the heat transfer coefficient converges as the number of grid cells increases. Grid 4 shows little difference (0.25% for water and 0.41% for HFE 7000) from the results obtained for Grid 4. Therefore, in the present study, Grid 4 is utilised for the numerical analysis.

Table 2 Grid independency test results

Grid number	**Number of cells in x direction**	**Number of cells in y direction**	**h (pure water)**	**h (pure HFE 7000)**
		Re = 800		
1	250	5	755.384	125.05
2	500	10	728.2	116.41
3	1000	20	720.32	114.63
4	**2000**	**40**	**718.47**	**114.16**
5	3000	40	719.26	114.21
		Re = 1600		
1	250	5	1120.64	158.05
2	500	10	1032.7	146.14
3	1000	20	1011.44	142.68
4	**2000**	**40**	**1006.25**	**141.86**
5	3000	40	1007.34	142

It is also important to ensure the appropriate grid cell size in order to obtain accurate simulation results. Therefore, y^+ value for Grid 4 is calculated and given in Table 3 at each Reynolds number. As it can be seen from Table 3 that y^+ in the laminar flow region at any Reynolds number remains less than 11.63 for Grid 4 [52, 53].

Table 3 y^+ values versus Reynolds number

Reynolds number	**Grid 4** (2000×40)
400	1.32
800	2.43
1200	3.47
1600	4.46

4.3. Validation of the computational model

Due to the absence of experimental and numerical studies for HFE 7000 based nanofluids, the experimental data of the local heat transfer coefficients of pure water and Al_2O_3/water nanofluid in laminar developing region represented by [54] was compared to the corresponding numerical results in order to validate the accuracy of the model. In the experimental work [54], a test rig was set-up in order to investigate the heat transfer characteristics of Al_2O_3/water nanofluid with particle sizes of 45 nm and 150 nm in a straight tube under constant heat flux conditions. The experimental test loop comprises a pump, a heated test section, a cooling section and a collecting tank. In the test section a straight tube with 4.75 mm inner diameter and 1200 mm long was utilised and constant heat flux was provided by wounding a Nickel-chrome wire that can give maximum power of 200W along the tube.

Figure 2 shows the comparison of the experimental heat transfer coefficient for both pure water and Al_2O_3/water nanofluid (with the particle diameter of 45nm and the volume concentration ratio of 4%) at Re = 1580 and Re = 1588 versus simulation results. It should be noted that the effect of various particle size was not considered in this study and the simulation results are only compared with the experimental results of Al_2O_3/water nanofluid with particle diameter of 45 nm as it is widely accepted that solid particles which have a diameter less than 100 nm can be easily fluidised and be treated as a single fluid.

As it is shown in Figure 2, the axial variation of the heat transfer coefficient using numerical results is in good agreement with the experimental data. The maximum discrepancy between the experimental data and numerical model is found to be 12%. As the heat transfer enhancement is highly related to the accuracy of the effective properties of nanofluid, namely thermal conductivity in homogenous model, several factors such as particle size, temperature dependent properties, random movement of particles and thermal dispersion, which might have an impact on the accurate determination of the effective thermal conductivity could be attributed to the reason of the deviation between the simulation and the experimental results [7, 55].

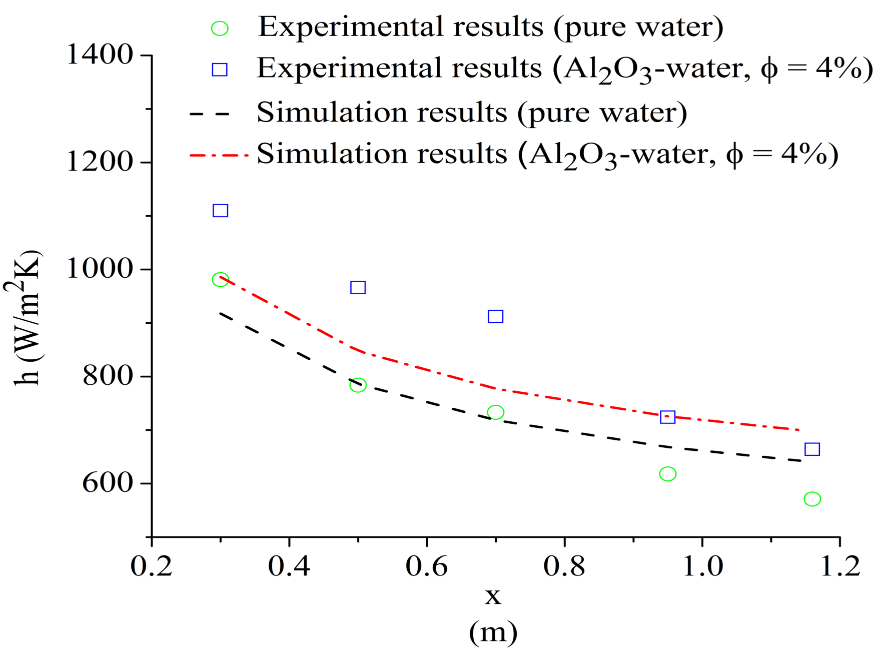

Figure 2 Comparison between the simulated and experimental results

5. Results and discussion

In this section, the simulations of Al_2O_3-HFE 7000, CuO-HFE 7000, SiO_2-HFE 7000 and MgO-HFE 7000 nanofluids at various Reynolds numbers (Re = 400-1600) and particle volume fraction (ϕ = 1-6%) under constant heat flux conditions were conducted and the effect of Reynolds number and particle volume concentration ratio of the nanofluids on the flow and heat transfer characteristics as well as the entropy generation is represented and discussed.

5.1. Temperature profiles

Figure 3 shows the axial bulk and wall temperature distributions of Al_2O_3-HFE 7000 nanofluids at Re = 800 and at ϕ = 0, 1, 4, 6%. It can be observed that increasing nanoparticle concentration decreases the temperature differences between the wall and bulk temperature of nanofluids. A similar trend is obtained in Ref. [40] for Al_2O_3-HFE 7100 with ϕ = 0 and 5%.

This behaviour of the wall and bulk temperatures shows the beneficial effects of the nanofluids in terms of having superior thermal properties in comparison to that of the base fluid which leads higher heat transfer coefficients consequently.

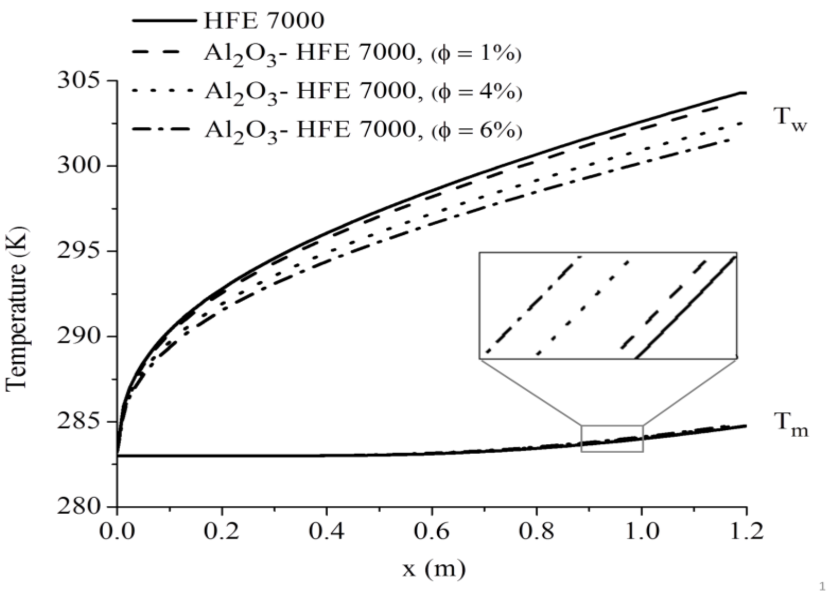

Figure 3 Axial distribution of wall and fluid temperature of Al_2O_3 nanofluid at various volume concentrations

The effect of particle volume concentration on the temperature distribution of Al_2O_3 - HFE 7000 nanofluids at Re = 800 is also represented in Figure 4.

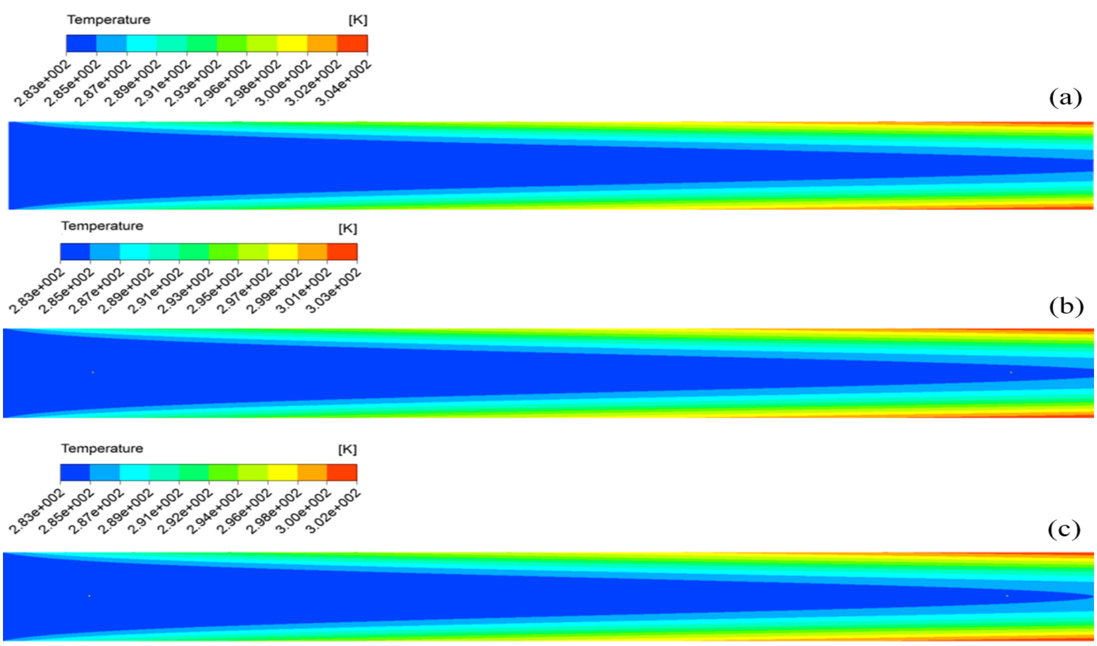

Figure 4 Temperature distribution of Al_2O_3-HFE 7000 nanofluids along the tube at a) 1% volume concentration b) 4% volume concentration c) 6% volume concentration

5.2. Convective heat transfer coefficient

Figure 5 illustrates the heat transfer coefficient of the investigated nanofluids and the base fluid at various Reynolds numbers and volumetric concentration ratio. It can be observed from Figure 5 that in general, the average heat transfer coefficient of each nanofluid is greater than the base fluid at any volumetric ratio and Reynolds number. The heat transfer coefficients of four nanofluids rise as the volume concentration ratio increases in the laminar flow regime. This is reasonable because the higher volume concentration ratios of nanoparticles lead a higher thermal conductivity in nanofluid than the conventional fluid which results in higher thermal-energy transfer. Similar findings were reported by previous researchers [17, 25, 36]. Among all the investigated nanofluids, MgO-HFE 7000 shows the highest heat transfer enhancement, at any given Reynolds number and particle volume fraction. For example, at Re = 400 and ϕ = 6% for the MgO-HFE 7000 nanofluid the enhancement in the heat transfer coefficient is approximately 17.5%, whereas for Al_2O_3-HFE 7000, CuO-HFE 7000 and SiO_2-HFE 7000, it is found to be 16.9%, 15.1% and 14.6% respectively.

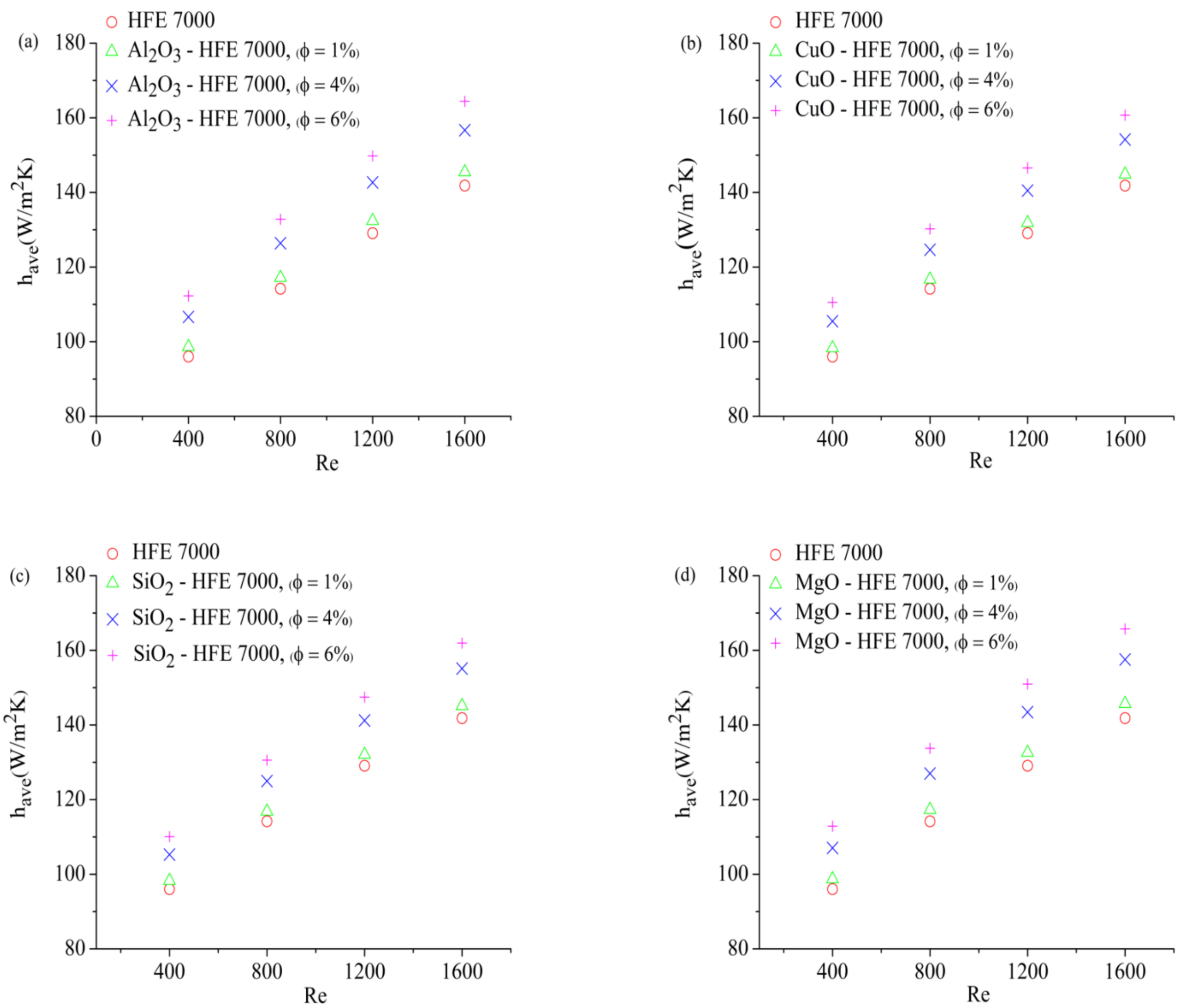

Figure 5 Variation of the heat transfer coefficients at different Reynolds number for (a) Al_2O_3-HFE 7000, (b) CuO-HFE 7000, (c) SiO_2-HFE 7000, (d) MgO-HFE 7000

This could be explained by the superior physical properties such as thermal conductivity of MgO compared to the other particles (Table 1**)**. As it is reported previously, in the single phase laminar flow model, the enhancement in the heat transfer coefficient of nanofluid is proportional to the increase in thermal conductivity of corresponding nanofluid [55]. This dependency of the heat transfer mechanism on the nanofluid effective properties might cause single-phase model to under-predict the heat transfer enhancement [24]. Alternatively, two phase models can be utilised in order to evaluate the heat transfer characteristics of nanofluids. However, they are more complicated and need higher computational cost [37]. In order to compare both the experimental results with the current model and two-phase models, it is necessary to conduct further theoretical study including two-phase models and experimental work.

5.3. *Pressure drop analysis*

It is also important to study the flow characteristics of nanofluids such as pressure drop in order to investigate their potential for practical applications [56]. Pressure drop within the tube at different Reynolds number and the volume concentration is demonstrated in Figure 6.

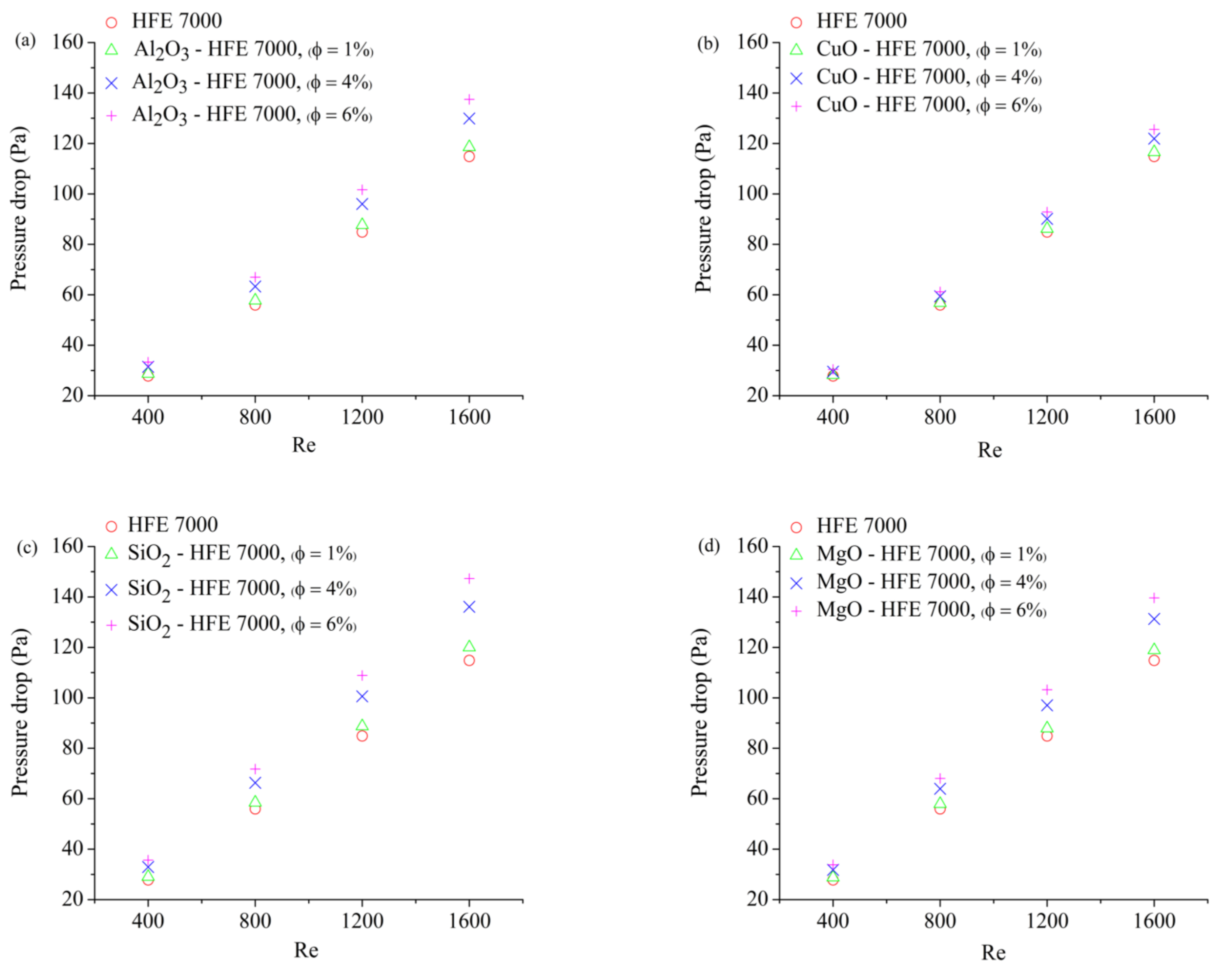

Figure 6 Variation of pressure drop at different Reynolds number for (a) Al_2O_3-HFE 7000, (b) CuO-HFE 7000, (c) SiO_2-HFE 7000, (d) MgO-HFE 7000

It is shown that pressure drop increases as the Reynolds number grows from 400 to 1600 and volume concentration from 1% to 6% for each nanofluid. The obtained results reveal that at Re = 1600 and ϕ = 6%, SiO_2-HFE 7000 nanofluid caused the highest enhancement in pressure drop (28.2%) among the four nanofluids. It is followed by MgO-HFE 7000 (21.5%),

Al_2O_3-HFE 7000 (19.7%) and CuO-HFE 7000 (9.3%). This is due to the fact that nanofluids become more viscous at higher volume concentration ratios which in turn results in higher pressure drop [18].

5.4. Entropy generation analysis

Entropy generation of the considered nanofluids in terms of irreversibility that was caused by thermal and frictional gradients with Reynolds number from 400 to 1600 and at four different volume fractions (0%, 1%, 4% and 6%) is demonstrated in Figure 7 and Figure 8.

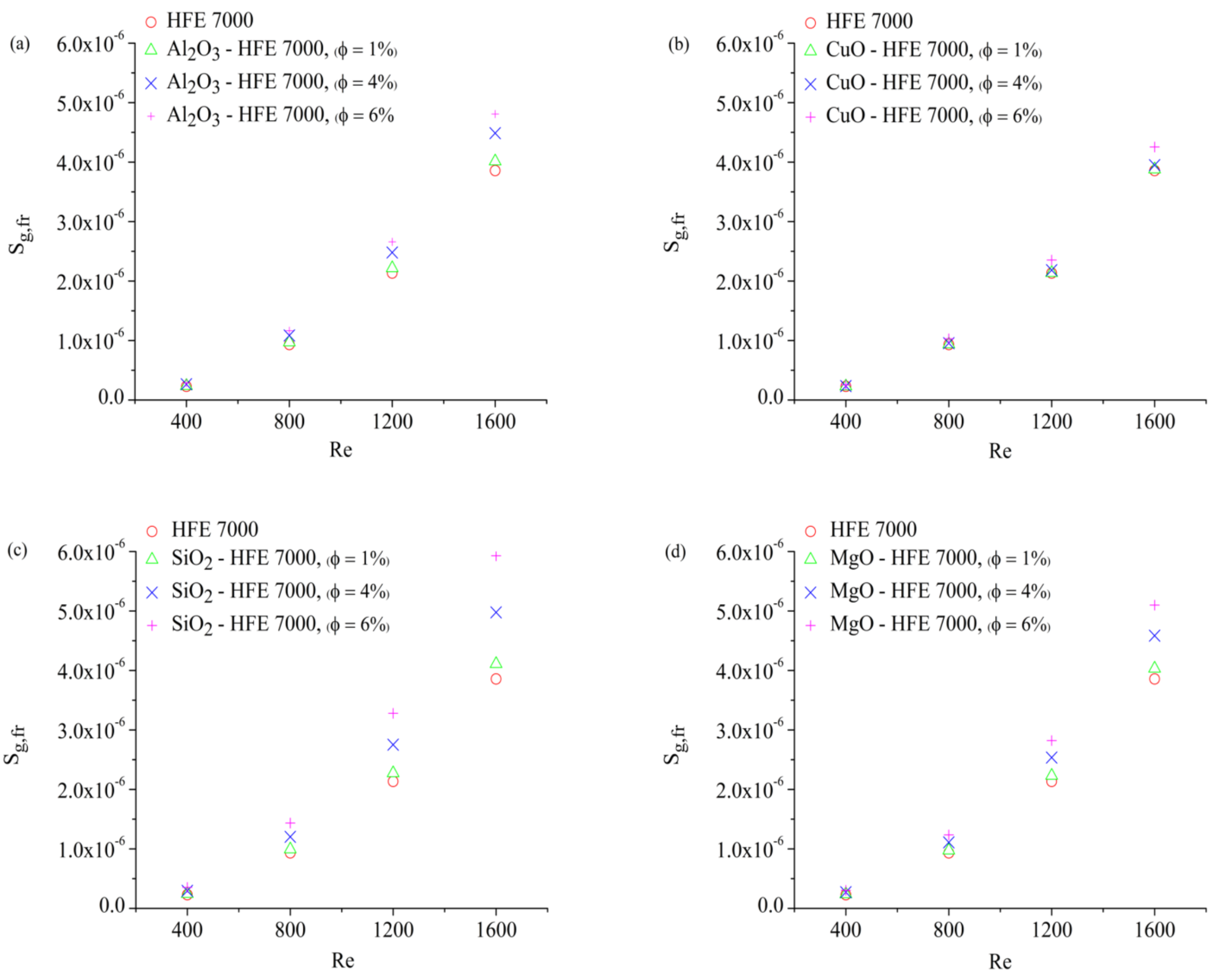

Figure 7 Variation of frictional entropy generation at different Reynolds number for (a) Al_2O_3-HFE 7000, (b) CuO-HFE 7000, (c) SiO_2-HFE 7000, (d) MgO-HFE 7000

It is visible from Figure 7 and Figure 8 that the growth in Reynolds number for both the base fluid and the nanofluids diminishes the thermal irreversibility whereas enhances the frictional entropy generation.

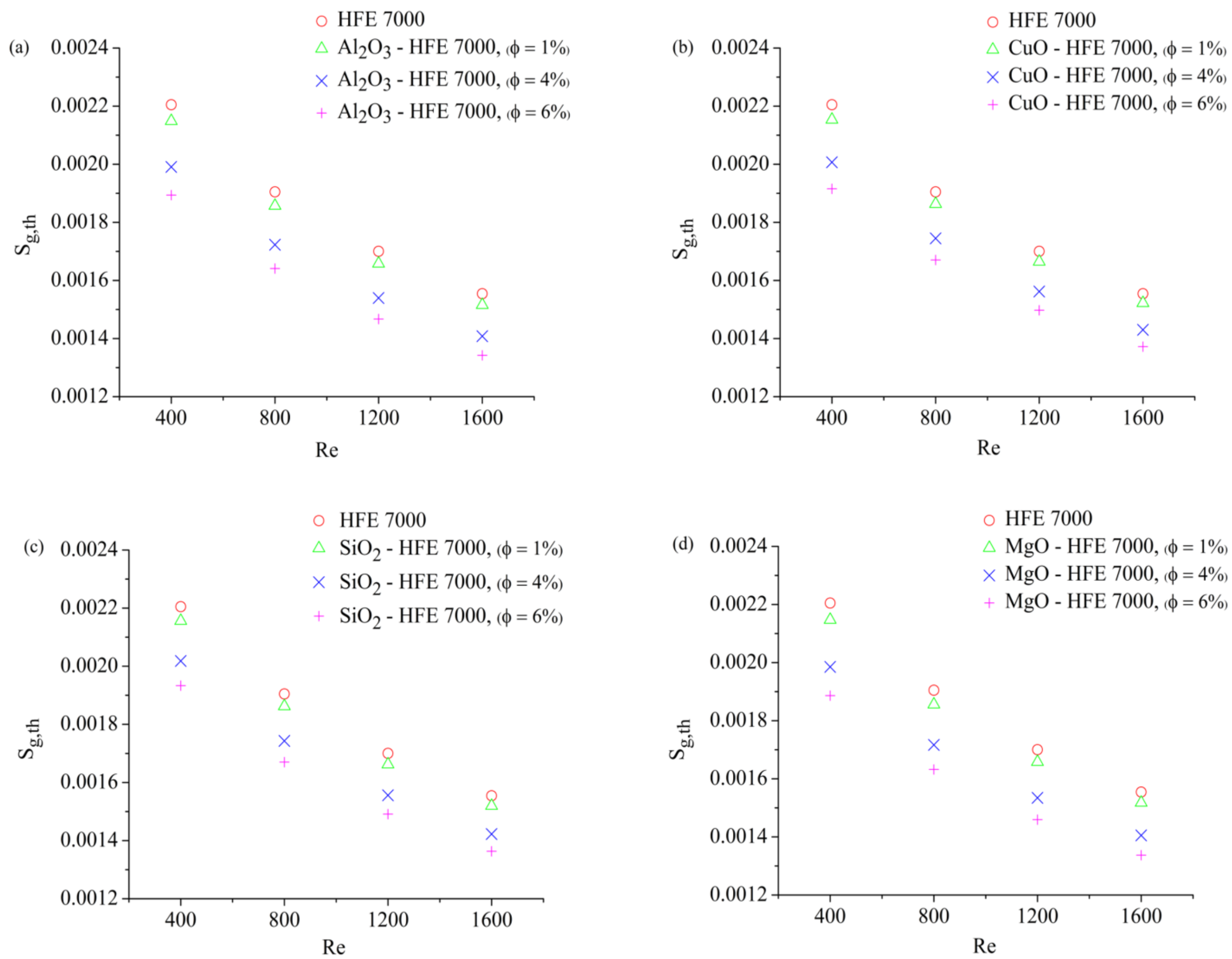

Figure 8 Variation of thermal entropy generation at different Reynolds number for (a) Al_2O_3-HFE 7000, (b) CuO-HFE 7000, (c) SiO_2-HFE 7000, (d) MgO-HFE 7000

The reason for that is the higher Reynolds number leads to a growth in the heat transfer coefficient. However, the higher velocity profile of the fluids at higher Reynolds number improves entropy generation due to the friction [33]. Similarly, the opposite trend between the thermal and frictional irreversibility for volume fraction can be found in Figure 7 and Figure 8. Namely, the thermal entropy generation diminishes with increasing volume concentration ratio. This can be explained by the fact that higher particle volume fraction leads higher nanofluid effective thermal conductivity and better heat transfer mechanism between the wall and the fluid which corresponds a decline in thermal dissipation and an improvement in the heat transfer mechanism. On the contrary, frictional entropy generation is increased with the volume concentration ratio. This is due to the growth of the viscosity of nanofluids as the nanoparticle volume fraction increases [28]. As it can be seen from Figure 7 and Figure 8 the magnitude of the thermal irreversibility is relatively higher than the irreversibility due to the friction.

In order to define the thermodynamic performance of the flow in terms of the second law efficiency the ratio of the total entropy generation of nanofluid to that of base fluid ($S_{gen,ratio}$) is defined as follows [35].

$$S_{gen,ratio} = \frac{S_{gen,tot,nf}}{S_{gen,tot,bf}} \tag{16}$$

where $S_{gen,tot,nf}$ and $S_{gen,tot,bf}$ represent the total entropy generation of the nanofluid and the base fluid respectively. As it is stated in Equation (16), $S_{gen,ratio}$ equals to 1 for pure HFE 7000 (ϕ = 0%) which shows that there is no contribution to entropy generation. Therefore, the lower the value of $S_{gen,ratio}$ the better the thermodynamic performance of the flow.

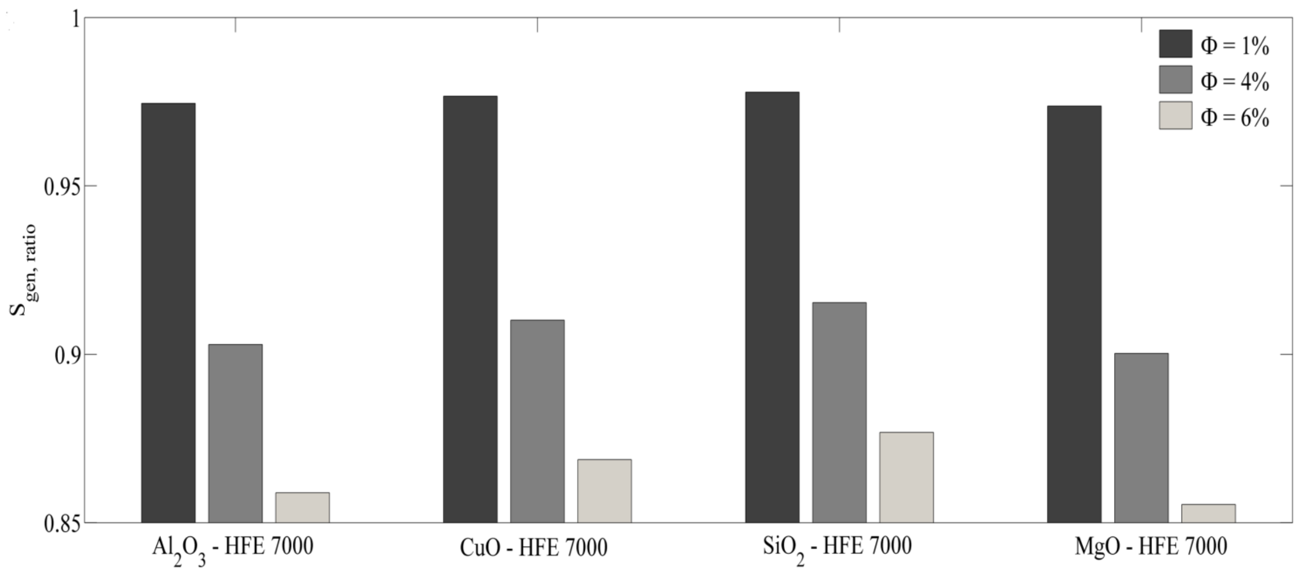

Figure 9 Entropy generation ratio of the nanofluids at Re = 800

Figure 9 indicates the entropy generation ratio of the investigated nanofluids for the volume concentration ratios. It can be highlighted from the figure that each nanofluid at any volume fraction has a lower value of the entropy generation rate in comparison to that of the base fluid ($S_{gen,ratio}$ = 1) which indicates the advantage of adding nanoparticles in terms of a reduction in total entropy generation. Additionally, the entropy generation rate decreases with increasing volume concentration and the decrease is more pronounced at 6% volume concentration ratio. For instance, the entropy generation rate drops from 0.97 to 0.85 and from 0.97 to 0.87 for MgO-HFE 7000 and SiO_2-HFE 7000 respectively as the volume concentration rises from 1% to 6%. This trend can be explained by the fact that higher volume concentration determines a reduction in thermal entropy generation. Although there is an opposite trend between the frictional and thermal entropy generation (Figure 7 and Figure 8) the effect of the former is relatively small compared to the latter. Thus, the overall behaviour of the total entropy generation is dominated by the thermal effects. Similar results were reported by [27, 31, 34] for Al_2O_3-water nanofluid. As a result, it can be concluded that the utilisation of Al_2O_3-HFE 7000, CuO-HFE 7000, SiO_2-HFE 7000 and MgO-HFE 7000 nanofluids is beneficial where the total entropy generation is dominated by the contribution of thermal irreversibility.

5.5. Correlations

Non-linear regression analysis is applied to the simulation results to derive the following correlations which can predict the average Nusselt number and friction factor for each investigated nanofluid. The evaluated equations are valid for $400 \leq Re \leq 1600$ and $0\% \leq \phi \leq 6\%$. The average Nusselt number is modelled as a function of Reynolds number, Prandtl number and volumetric concentration ratio whereas friction factor as a function of Reynolds number and volumetric concentration ratio.

Nusselt number

Al_2O_3-HFE 7000: $$Nu_{ave} = 0.576(Re\,Pr)^{0.28}(1+\phi)^{3.016} \quad (17)$$

CuO-HFE 7000: $$Nu_{ave} = 0.591(Re\,Pr)^{0.278}(1+\phi)^{2.658} \quad (18)$$

SiO_2-HFE 7000: $$Nu_{ave} = 0.567(Re\,Pr)^{0.282}(1+\phi)^{2.737} \quad (19)$$

MgO-HFE 7000: $$Nu_{ave} = 0.571(Re\,Pr)^{0.281}(1+\phi)^{3.143} \quad (20)$$

Friction factor

Al_2O_3-HFE 7000: $f = 48.492Re^{-0.984}(1+\phi)^{0.033}$ (21)

CuO-HFE 7000: $f = 48.197Re^{-0.984}(1+\phi)^{0.899}$ (22)

SiO_2-HFE 7000: $f = 48.696Re^{-0.984}(1+\phi)^{0.401}$ (23)

MgO-HFE 7000: $f = 48.056Re^{-0.983}(1+\phi)^{0.398}$ (24)

The maximum deviation between the simulated and the predicted results are found to be 1.74% and 3% for Nusselt number and friction factor of CuO-HFE 7000 nanofluid respectively.

6. Conclusions

This paper investigates the convective heat transfer, pressure drop and entropy generation characteristics of HFE-7000 based Al_2O_3, CuO, SiO_2 and MgO nanofluids, using the single phase approach in a circular tube with constant heat flux boundary conditions in laminar flow region. It was found that the inclusion of nanoparticles (Al_2O_3, CuO, SiO_2 and MgO) increased the heat transfer coefficient (2.1% – 17.5%). This augmentation is attributed to the enhancement in the thermal conductivity of nanofluids. However, heat transfer enhancement is accompanied by increasing viscosity as well as an increase in pressure drop (1.5% – 28.2%). The enhancement in heat transfer and pressure drop found to be more pronounced with the increase in particle concentration and Reynolds number. Entropy generation results also demonstrated that when operating with constant Reynolds number, the thermal entropy generation tends to decrease whereas the frictional entropy generation tends to increase for each investigated nanofluid. However, using nanofluids caused a lower total entropy generation due to the superior contribution of thermal entropy generation compared to the frictional entropy generation. It can be concluded that in the laminar flow regime, for any Reynolds number adding nanoparticles of Al_2O_3, CuO, SiO_2 and MgO into the HFE 7000 is beneficial where the contribution of fluid friction is adequately less than the contribution of heat transfer to the total entropy generation of the flow. Finally, the current research provides a guideline to heat transfer applications on nano additives for enhanced thermal efficiency of solar thermal systems. Overall, this contribution will bring significant impacts to renewable energy technology research and development where novel and environmentally friendly thermo-fluids have been deployed.

Acknowledgement

The authors would like to acknowledge and thank Future Energy Source (FES) Ltd for providing full funding and technological support to conduct this research.

References

[1] W. Duangthongsuk, S. Wongwises, Heat transfer enhancement and pressure drop characteristics of TiO 2–water nanofluid in a double-tube counter flow heat exchanger, International Journal of Heat and Mass Transfer, 52(7) (2009) 2059-2067.
[2] A. Behzadmehr, M. Saffar-Avval, N. Galanis, Prediction of turbulent forced convection of a nanofluid in a tube with uniform heat flux using a two phase approach, International Journal of Heat and Fluid Flow, 28(2) (2007) 211-219.
[3] M. Chandrasekar, S. Suresh, Experiments to explore the mechanisms of heat transfer in nanocrystalline alumina/water nanofluid under laminar and turbulent flow conditions, Experimental Heat Transfer, 24(3) (2011) 234-256.
[4] M. Hejazian, M.K. Moraveji, A. Beheshti, Comparative study of Euler and mixture models for turbulent flow of Al 2 O 3 nanofluid inside a horizontal tube, International Communications in Heat and Mass Transfer, 52 (2014) 152-158.
[5] Z. Khan, Z. Khan, A. Ghafoor, A review of performance enhancement of PCM based latent heat storage system within the context of materials, thermal stability and compatibility, Energy Conversion and Management, 115 (2016) 132-158.
[6] W. Minkowycz, E.M. Sparrow, J.P. Abraham, Nanoparticle Heat Transfer and Fluid Flow, CRC press, 2012.
[7] Y. Xuan, Q. Li, Heat transfer enhancement of nanofluids, International Journal of heat and fluid flow, 21(1) (2000) 58-64.
[8] J.A. Eastman, S. Choi, S. Li, W. Yu, L. Thompson, Anomalously increased effective thermal conductivities of ethylene glycol-based nanofluids containing copper nanoparticles, Applied physics letters, 78(6) (2001) 718-720.
[9] M. Assael, C.-F. Chen, I. Metaxa, W. Wakeham, Thermal conductivity of suspensions of carbon nanotubes in water, International Journal of Thermophysics, 25(4) (2004) 971-985.
[10] J.-H. Lee, K.S. Hwang, S.P. Jang, B.H. Lee, J.H. Kim, S.U. Choi, C.J. Choi, Effective viscosities and thermal conductivities of aqueous nanofluids containing low volume concentrations of Al 2 O 3 nanoparticles, International Journal of Heat and Mass Transfer, 51(11) (2008) 2651-2656.
[11] L. Godson, B. Raja, D.M. Lal, S. Wongwises, Experimental investigation on the thermal conductivity and viscosity of silver-deionized water nanofluid, Experimental Heat Transfer, 23(4) (2010) 317-332.
[12] W. Yu, H. Xie, L. Chen, Y. Li, Investigation on the thermal transport properties of ethylene glycol-based nanofluids containing copper nanoparticles, Powder Technology, 197(3) (2010) 218-221.
[13] P. Sharma, I.-H. Baek, T. Cho, S. Park, K.B. Lee, Enhancement of thermal conductivity of ethylene glycol based silver nanofluids, Powder technology, 208(1) (2011) 7-19.
[14] S. Kakaç, A. Pramuanjaroenkij, Single-phase and two-phase treatments of convective heat transfer enhancement with nanofluids–A state-of-the-art review, International Journal of Thermal Sciences, 100 (2016) 75-97.
[15] D. Wen, Y. Ding, Experimental investigation into convective heat transfer of nanofluids at the entrance region under laminar flow conditions, International journal of heat and mass transfer, 47(24) (2004) 5181-5188.
[16] S. Zeinali Heris, S.G. Etemad, M. Nasr Esfahany, Experimental investigation of oxide nanofluids laminar flow convective heat transfer, International Communications in Heat and Mass Transfer, 33(4) (2006) 529-535.
[17] M.K. Moraveji, M. Darabi, S.M.H. Haddad, R. Davarnejad, Modeling of convective heat transfer of a nanofluid in the developing region of tube flow with computational fluid

dynamics, International Communications in Heat and Mass Transfer, 38(9) (2011) 1291-1295.

[18] H. Demir, A. Dalkilic, N. Kürekci, W. Duangthongsuk, S. Wongwises, Numerical investigation on the single phase forced convection heat transfer characteristics of TiO 2 nanofluids in a double-tube counter flow heat exchanger, International Communications in Heat and Mass Transfer, 38(2) (2011) 218-228.

[19] B. Salman, H. Mohammed, A.S. Kherbeet, Numerical and experimental investigation of heat transfer enhancement in a microtube using nanofluids, International Communications in Heat and Mass Transfer, 59 (2014) 88-100.

[20] S. Zeinali Heris, A. Kazemi-Beydokhti, S. Noie, S. Rezvan, Numerical study on convective heat transfer of Al2O3/water, CuO/water and Cu/water nanofluids through square cross-section duct in laminar flow, Engineering Applications of Computational Fluid Mechanics, 6(1) (2012) 1-14.

[21] S.Z. Heris, M.N. Esfahany, G. Etemad, Numerical investigation of nanofluid laminar convective heat transfer through a circular tube, Numerical Heat Transfer, Part A: Applications, 52(11) (2007) 1043-1058.

[22] S. Göktepe, K. Atalık, H. Ertürk, Comparison of single and two-phase models for nanofluid convection at the entrance of a uniformly heated tube, International Journal of Thermal Sciences, 80 (2014) 83-92.

[23] M.H. Fard, M.N. Esfahany, M. Talaie, Numerical study of convective heat transfer of nanofluids in a circular tube two-phase model versus single-phase model, International Communications in Heat and Mass Transfer, 37(1) (2010) 91-97.

[24] M. Kalteh, A. Abbassi, M. Saffar-Avval, J. Harting, Eulerian–Eulerian two-phase numerical simulation of nanofluid laminar forced convection in a microchannel, International journal of heat and fluid flow, 32(1) (2011) 107-116.

[25] M.K. Moraveji, R.M. Ardehali, CFD modeling (comparing single and two-phase approaches) on thermal performance of Al 2 O 3/water nanofluid in mini-channel heat sink, International Communications in Heat and Mass Transfer, 44 (2013) 157-164.

[26] Y.-j. Chen, Y.-y. Li, Z.-h. Liu, Numerical simulations of forced convection heat transfer and flow characteristics of nanofluids in small tubes using two-phase models, International Journal of Heat and Mass Transfer, 78 (2014) 993-1003.

[27] M. Moghaddami, S. Shahidi, M. Siavashi, Entropy generation analysis of nanofluid flow in turbulent and laminar regimes, Journal of Computational and Theoretical Nanoscience, 9(10) (2012) 1586-1595.

[28] V. Biancoa, O. Mancab, S. Nardini, Entropy generation analysis of turbulent convection flow of Al 2 O 3–water nanofluid in a circular tube subjected to constant wall heat flux, Energy Convers Manage, 77 (2014) 306-314.

[29] O. Mahian, A. Kianifar, C. Kleinstreuer, A.-N. Moh'd A, I. Pop, A.Z. Sahin, S. Wongwises, A review of entropy generation in nanofluid flow, International Journal of Heat and Mass Transfer, 65 (2013) 514-532.

[30] P.K. Singh, K. Anoop, T. Sundararajan, S.K. Das, Entropy generation due to flow and heat transfer in nanofluids, International Journal of Heat and Mass Transfer, 53(21) (2010) 4757-4767.

[31] M. Moghaddami, A. Mohammadzade, S.A.V. Esfehani, Second law analysis of nanofluid flow, Energy Conversion and Management, 52(2) (2011) 1397-1405.

[32] A. Shalchi-Tabrizi, H.R. Seyf, Analysis of entropy generation and convective heat transfer of Al 2 O 3 nanofluid flow in a tangential micro heat sink, International Journal of Heat and Mass Transfer, 55(15) (2012) 4366-4375.

[33] G. Saha, M.C. Paul, Heat transfer and entropy generation of turbulent forced convection flow of nanofluids in a heated pipe, International Communications in Heat and Mass Transfer, 61 (2015) 26-36.

[34] N. Zhao, J. Yang, H. Li, Z. Zhang, S. Li, Numerical investigations of laminar heat transfer and flow performance of Al 2 O 3–water nanofluids in a flat tube, International Journal of Heat and Mass Transfer, 92 (2016) 268-282.

[35] M. Siavashi, M. Jamali, Heat transfer and entropy generation analysis of turbulent flow of TiO 2-water nanofluid inside annuli with different radius ratios using two-phase mixture model, Applied Thermal Engineering, 100 (2016) 1149-1160.

[36] N. Purohit, V.A. Purohit, K. Purohit, Assessment of nanofluids for laminar convective heat transfer: A numerical study, Engineering Science and Technology, an International Journal, (2015).

[37] A. Ebrahimi, F. Rikhtegar, A. Sabaghan, E. Roohi, Heat transfer and entropy generation in a microchannel with longitudinal vortex generators using nanofluids, Energy, 101 (2016) 190-201.

[38] W.-T. Tsai, Environmental risk assessment of hydrofluoroethers (HFEs), Journal of hazardous materials, 119(1) (2005) 69-78.

[39] J. Lee, I. Mudawar, Assessment of the effectiveness of nanofluids for single-phase and two-phase heat transfer in micro-channels, International Journal of Heat and Mass Transfer, 50(3) (2007) 452-463.

[40] T. Bergman, Effect of reduced specific heats of nanofluids on single phase, laminar internal forced convection, International Journal of heat and mass Transfer, 52(5) (2009) 1240-1244.

[41] R. Ellahi, M. Hassan, A. Zeeshan, A.A. Khan, The shape effects of nanoparticles suspended in HFE-7100 over wedge with entropy generation and mixed convection, Applied Nanoscience, (2015) 1-11.

[42] H. Helvaci, Z.A. Khan, Mathematical modelling and simulation of multiphase flow in a flat plate solar energy collector, Energy Conversion and Management, 106 (2015) 139-150.

[43] H.U. Helvaci, Z.A. Khan, Experimental study of thermodynamic assessment of a small scale solar thermal system, Energy Conversion and Management, 117 (2016) 567-576.

[44] B.C. Pak, Y.I. Cho, Hydrodynamic and heat transfer study of dispersed fluids with submicron metallic oxide particles, Experimental Heat Transfer an International Journal, 11(2) (1998) 151-170.

[45] R. Hamilton, O. Crosser, Thermal conductivity of heterogeneous two-component systems, Industrial & Engineering chemistry fundamentals, 1(3) (1962) 187-191.

[46] A. Einstein, Eine neue bestimmung der moleküldimensionen, Annalen der Physik, 324(2) (1906) 289-306.

[47] R. Davarnejad, M. Jamshidzadeh, CFD modeling of heat transfer performance of MgO-water nanofluid under turbulent flow, Engineering Science and Technology, an International Journal, 18(4) (2015) 536-542.

[48] E. Lemmon, M. Huber, M. McLinden, NIST reference database 23: reference fluid thermodynamic and transport properties-REFPROP, version 9.1, Standard Reference Data Program, (2013).

[49] G. Pathipakka, P. Sivashanmugam, Heat transfer behaviour of nanofluids in a uniformly heated circular tube fitted with helical inserts in laminar flow, Superlattices and Microstructures, 47(2) (2010) 349-360.

[50] R. Nasrin, M. Alim, Performance of nanofluids on heat transfer in a wavy solar collector, International Journal of Engineering, Science and Technology, 5(3) (2013) 58-77.

[51] A.F.U.s. Guide, Release 15.0, ANSYS, Inc.: Canonsburg, PA, (2013).

[52] H.K. Versteeg, W. Malalasekera, An introduction to computational fluid dynamics: the finite volume method, Pearson Education, 2007.
[53] H. Ingason, Y.Z. Li, A. Lönnermark, Tunnel fire dynamics, Springer, 2014.
[54] K. Anoop, T. Sundararajan, S.K. Das, Effect of particle size on the convective heat transfer in nanofluid in the developing region, International journal of heat and mass transfer, 52(9) (2009) 2189-2195.
[55] V. Bianco, F. Chiacchio, O. Manca, S. Nardini, Numerical investigation of nanofluids forced convection in circular tubes, Applied Thermal Engineering, 29(17) (2009) 3632-3642.
[56] M. Heyhat, F. Kowsary, A. Rashidi, M. Momenpour, A. Amrollahi, Experimental investigation of laminar convective heat transfer and pressure drop of water-based Al 2 O 3 nanofluids in fully developed flow regime, Experimental Thermal and Fluid Science, 44 (2013) 483-489.

Table captions

Table 1 Thermo-physical properties of the base fluids (water and HFE 7000) and the nanoparticles

Table 2 Grid independency test results

Table 3 y^+ values versus Reynolds number

Figure captions

Figure 1 Schematic of the flow domain under consideration

Figure 2 Comparison between the simulated and experimental results

Figure 3 Axial distribution of wall and fluid temperature of Al_2O_3 nanofluid at various volume concentrations

Figure 4 Temperature distribution of Al_2O_3-HFE 7000 nanofluids along the tube at a) 1% volume concentration b) 4% volume concentration c) 6% volume concentration

Figure 5 Variation of the heat transfer coefficients at different Reynolds number for (a) Al_2O_3-HFE 7000, (b) CuO-HFE 7000, (c) SiO_2-HFE 7000, (d) MgO-HFE 7000

Figure 6 Variation of pressure drop at different Reynolds number for (a) Al_2O_3-HFE 7000, (b) CuO-HFE 7000, (c) SiO_2-HFE 7000, (d) MgO-HFE 7000

Figure 7 Variation of frictional entropy generation at different Reynolds number for (a) Al_2O_3-HFE 7000, (b) CuO-HFE 7000, (c) SiO_2-HFE 7000, (d) MgO-HFE 7000

Figure 8 Variation of thermal entropy generation at different Reynolds number for (a) Al_2O_3-HFE 7000, (b) CuO-HFE 7000, (c) SiO_2-HFE 7000, (d) MgO-HFE 7000

Figure 9 Entropy generation ratio of the nanofluids at Re = 800